Experimental Time-Domain Study for Bandpass Negative Group Delay Analysis With Lill-Shape Microstrip Circuit

Remy Vauche, Rym Assila Belhadj Mefteh, Fayrouz Haddad, Jamel Nebhen, Wenceslas Rahajandraibe, Fayu Wan, Sebastien Lallechere, Blaise Ravelo

IEEE Access
Multidisciplinary ⋮ Rapid Review ⋮ Open Access Journal

Received January 18, 2021, accepted January 29, 2021, date of publication February 1, 2021, date of current version February 10, 2021.

Digital Object Identifier 10.1109/ACCESS.2021.3056221

Experimental Time-Domain Study for Bandpass Negative Group Delay Analysis With Lill-Shape Microstrip Circuit

RÉMY VAUCHÉ[1], (Member, IEEE), RYM ASSILA BELHADJ MEFTEH[1], FAYROUZ HADDAD[1], (Member, IEEE), JAMEL NEBHEN[2], (Member, IEEE), WENCESLAS RAHAJANDRAIBE[1], (Member, IEEE), FAYU WAN[3], (Member, IEEE), SÉBASTIEN LALLÉCHÈRE[4], (Member, IEEE), AND BLAISE RAVELO[3], (Member, IEEE)

[1]Aix Marseille University, Université de Toulon, CNRS, IM2NP, 13397 Marseille, France
[2]College of Computer Science and Engineering, Prince Sattam bin Abdulaziz University, Alkharj 11942, Saudi Arabia
[3]School of Electronic and Information Engineering, Nanjing University of Information Science & Technology, Nanjing 210044, China
[4]Institut Pascal, Sigma Clermont, Université Clermont Auvergne, 63000 Clermont-Ferrand, France

Corresponding author: Blaise Ravelo (blaise.ravelo@nuist.edu.cn)

This work was supported in part by NSFC under Grant 61601233 and Grant 61750110535, in part by NSF of Jiangsu under Grant BK20150918, in part by the Jiangsu Innovation and Enterprise Group Talents Plan 2015 under Grant SRCB201526, in part by Priority Academic Program Development (PAPD), and in part by the Deanship of Scientific Research at Prince Sattam Bin Abdulaziz University, Saudi Arabia.

ABSTRACT This paper focuses on the time-domain analysis of bandpass (BP) negative group delay (NGD) function. The innovative NGD investigation is based on the time-domain experimentation of an innovative topology of ''lill''-shape passive microstrip circuit. The design principle of the proof of concept (POC) constituted by particular microstrip shapes is described. The NGD circuit is inspired from a recent fully distributed ''li''-topology. Before the time-domain investigation, the BP NGD specifications of the circuit under study are academically defined. As practical application of the basic definition, a frequency domain validation of ''lill''-circuit is presented in the first section of the paper. The POC circuit is specified by a −8 ns NGD value at 2.31 GHz NGD center frequency and a 27 MHz NGD bandwidth. The ''lill''-circuit exhibits an attenuation loss of about −6.2 dB at the NGD center frequency. Then, the two-port black box model of ''lill''-NGD-circuit represented by touchstone data of the measured S-parameters is exploited for the transient simulation. The measured group delay (GD) illustrates that the tested ''lill''-circuit operates as a BP function regarding the NGD with NGD equal to −8.1 ns at the NGD center frequency. The time-domain demonstration of the BP NGD function was performed using a gaussian pulse modulating sine carrier. The innovative experimental setup with the possibility to plot simultaneously well synchronized input and output signals is explained. The BP NGD time-domain response is understood from commercial tool simulation using the touchstone S-parameters of the measured ''lill''-circuit by using a Gaussian up-converted pulse having a 27 MHz frequency bandwidth. It was observed that the output signals are delayed when the sine carrier is out of NGD-band. However, the output signal envelope is in advanced of about −8 ns when the carrier is tuned to be approximately equal to the 2.31 GHz NGD center frequency. To confirm the time-domain typical behavior of BP NGD response, an input pulse signal having Gaussian waveform were considered during the test. However, the input signal spectrum must be determined in function of the NGD bandwidth. After tests, measured output signal envelopes presenting leading edge, trailing edge and peak in time-advance compared to the input ones are observed experimentally. The results of the present feasibility study open a potential microwave communication application of BP NGD function notably for systems operating with ISM and IEEE 802.11 standards.

INDEX TERMS Bandpass (BP) negative group delay (NGD), S-parameters, time-domain experimentation, Gaussian pulse, time-advance, microstrip circuit, transient analysis, microwave circuit, measurement technique.

The associate editor coordinating the review of this manuscript and approving it for publication was Wenjie Feng.

I. INTRODUCTION

Recent studies featured some tentative RF and microwave applications of unfamiliar negative group delay (NGD) circuits [1]–[5]. The NGD circuits are expected to be useful for the improvement of certain microwave devices as antenna [1], for the design of non-Foster reactive elements [2], [3], and group delay (GD) equalization techniques [4], [5]. But these NGD circuits applications are still less exploited compared to the other classical microwave circuits as filters, antennas, amplifiers and so one. This fact can be explained due to the misunderstanding and the counterintuitive aspect of the NGD function. Therefore, more illustrative and more understandable principle of NGD concept needs to be proposed.

The microwave NGD effect can be historically explained from the research works performed by optical researchers some decades ago [6], [7]. The NGD effect and the causality constitutes the kernel of questions between the scientific. The existence, understandability, and the interpretation of the NGD effect become one of controversy topic of physicists and engineers. To close the scientific controversy, large efforts during several decades must be considered. Indeed, experimental investigations confirmed the feasibility of the NGD effect with pulse signal propagation through negative group velocity (NGV) medium [6], [7]. The effect was, thus, verified with negative refractive index (NRI) artificial metamaterials [8], [9]. Thanks to the transfer function equivalence, microwave NGD circuits were designed and experimented [8], [10].

Then, brave research teams [11]–[19] fascinated by the counterintuitive effect of the NGD function were attracted to the problem of low-attenuation and compact NGD circuits design. To overcome the attenuation loss, active NGD circuits [14], [19], [20] were designed and experimented. It has been found since the early of 2000s that innumerable microwave circuit topologies [8]–[26] are susceptible to behave as an NGD function. In 2010s, one of the most explored NGD circuits are based on the microstrip transmission line (TL) [8], [9], [15]–[17], [21]–[23]. Among the TL-based NGD topologies, the circuits designed with coupled-line (CL) ones [22]–[24] seem to be the best candidate against the issues related to the attenuation loss. Until now, the degree of freedom of topologies using CL structure motivates the NGD researchers to exploit the structure.

Despite the progressive development of the research works on the NGD circuit design [8]–[24], the NGD functions are not still open to most of non-specialist electronic design, fabrication and sale engineers. Many questions remain technically open about the meaning and the interpretation of the NGD effect. The design method of microwave NGD circuits are not easy for non-specialist engineers. To illuminate further such technical darkness, a new approach of NGD theory based on an analogy between NGD circuits and filters was initiated [21]. This led to the definition of the original concept of low-pass and bandpass (BP) NGD function. However, in difference to the filter response, the NGD classification depends on the sign of the GD. Using this innovative concept, it is possible to classify all the microwave and optical NGD circuits [1]–[24] as BP NGD function. In addition to the NGD classification, the most rational explanation of the NGD effect remains on the time-domain investigation [25], [26]. But compared to the classical functions in the communication engineering, especially, on the ultra-wide band (UWB) testing [27]–[33], a very little research work is available in the literature on the BP NGD function experimentation in the time-domain [25], [26]. Most of the existing works are limited to the plots of GD from the transmission parameters.

To overcome this technical bottleneck, it is proposed in the present paper to investigate innovatively on the analysis in the time-domain of BP NGD circuits. It is expected to exploit the empirical approach on the transient short duration voltage [27], [28], real-time impedance measurements [29] and also assessment of time-averaged realistic maximum power levels from microwave signal transmission [30], [31]. The main novelty of the present research works is on the consideration of typical UWB pulse generations for emulating the input transient signals [32], [33]. Indeed, this measurement technique was rarely applied to the BP NGD circuit. However, a pioneer research work is hopefully proposed in the present paper and introduces also an innovative NGD passive topology.

The paper is organized in five different sections as follows:

- Section II defines the basic theory of BP NGD function. First, the GD expression from the two-port S-matrix is recalled. Then, the ideal diagram of BP NGD response is described. The main specifications of BP NGD function are defined.
- Section III is the design description of the innovative ''lill''-circuit topology. The design and the implementation of the circuit in microstrip technology is introduced. Then, the validation BP NGD behavior is discussed based on the S-parameter measurement.
- Section IV addresses the general principle of the time-domain investigation of BP NGD circuits. The principle is illustrated using simulation of black box model based on frequency domain measurement results.
- Section V explores more importantly the time-domain validation of BP NGD functions considering the ''lill''-circuit prototype. The experimental setup of the BP NGD time-domain measurement is explained. Then, a discussion is made on the measurement results based on the comparison between the intriguing behaviors of input and output signals.
- Then, Section VI ends the paper with the final conclusion.

II. RECALL ON UNFAMILIAR BP NGD FUNCTION

To design a microwave NGD circuit, we proceed generally with the S-matrix approach. The present section will introduce the general presentation of two-port circuit S-matrix.

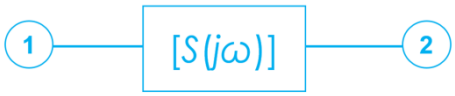

FIGURE 1. Two-port general system.

Then, the main specifications of ideal BP NGD response will be defined.

A. S-MATRIX APPROACH

Fig. 1 represents the general block diagram of two-port circuit as a S-matrix system. By denoting the Laplace variable by:

$$s = j\omega = j2\pi f \tag{1}$$

in function of angular frequency ω for the case of symmetric passive circuit, a two-port S-matrix is analytically represented by:

$$[S(s)] = \begin{bmatrix} S_{11}(s) & S_{21}(s) \\ S_{21}(s) & S_{11}(s) \end{bmatrix}. \tag{2}$$

The unfamiliar BP NGD analysis is generally performed as classical microwave function as filters, amplifier, or other by paying more attention on the GD response. For the classical system, the main parameters of study are:

- the reflection parameter magnitude:

$$S_{11}(\omega) = |S_{11}(j\omega)| \tag{3}$$

- the transmission parameter magnitude:

$$S_{21}(\omega) = |S_{21}(j\omega)| \tag{4}$$

In addition to the classical parameters, the study requires more focus on the GD response. For this reason, to realize the analysis, the following frequency domain responses are needed:

- the phase of the transmission coefficient which is defined by:

$$\varphi(\omega) = \arg\left[S_{21}(j\omega)\right] \tag{5}$$

- the frequency dependent GD response which is defined by:

$$GD(\omega) = -\frac{\partial\varphi(\omega)}{\partial\omega}. \tag{6}$$

In most of ordinary microwave functions, this GD is naturally positive and expresses the propagation delay of a modulated signal through the communication system. However, the main particularity of this research work is to try to explain using an easier way, the existence of the GD with negative value in all aspects. By exploiting this GD, it is possible specify the main parameters of a BP NGD function as introduced in the following subsection.

B. INTRODUCTION ON THE BP NGD FUNCTION SPECIFICATIONS

As initial step of the NGD circuit design, the desired specifications must be chosen. For the full understanding, an introduction of basic BP NGD specification is usually needed before the exploration of real circuits.

1) EXISTENCE CONDION OF NGD FUNCTION

First and foremost, the existence of NGD function for the two-port system shown in Fig. 1 is mathematically equivalent to the possibility to obtain the condition:

$$GD(\omega) < 0. \tag{7}$$

This analytical representation is equivalent to find an angular frequency band where the GD becomes negative. In this case, the NGD cut-off frequencies can be defined as the roots of equation:

$$GD(\omega) = 0. \tag{8}$$

If positive real roots exist, it can be assumed that the NGD bandwidth:

$$\Delta\omega = 2\pi\,\Delta f \tag{9}$$

is the difference between two successive NGD cut-off frequencies if the GD is negative for the frequencies between them.

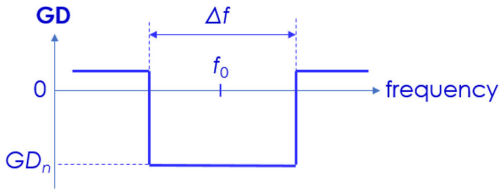

FIGURE 2. BP NGD ideal response.

2) IDEAL FREQUENCY RESPONSE OF BP NGD FUNCTION

A completely ideal response of BP NGD function can be represented by the graph shown in Fig. 2. This ideal diagram serves to clearly define the desired specifications before the BP NGD circuit design with the constraint characterized by:

- the NGD center angular frequency:

$$\omega_0 = 2\pi f_0, \tag{10}$$

- the NGD value corresponding to the NGD center frequency:

$$GD(\omega_0) = GD_n < 0. \tag{11}$$

- the NGD cut-off angular frequencies:

$$\begin{cases} \omega_1 = 2\pi f_1 \\ \omega_2 = 2\pi f_2 \end{cases} \tag{12}$$

which corresponds to the following analytical relation for the ideal diagram of Fig. 2:

$$GD_n = GD(\omega) \leq 0 \text{for} \omega_1 \leq \omega \leq \omega_2. \tag{13}$$

- the NGD bandwidth which is delimited by the NGD cut-off frequencies:

$$\Delta\omega = \omega_2 - \omega_1. \tag{14}$$

In addition to the GD response, the BP NGD analysis must also be performed by taking into account the transmission coefficient. Saying this, the next paragraph will specify briefly what is expected for the transmission coefficient magnitude.

3) TRANSMISSION COEFFICIENT MAGNITUDE

Similar to the filter design, the NGD circuit transmission coefficient should be defined in function of the targeted application. To take into account to this parameter, the transmission coefficient magnitude constraint may be added among the NGD circuit specifications. This specification can be formulated by the relation:

$$S_{21}(\omega_0) = A. \tag{15}$$

For the case of passive circuits, the transmission coefficient magnitude must be a real positive lower than unity:

$$0 < A < 1. \tag{16}$$

The following section focuses on a practical example of BP NGD circuit with a particular shape microstrip structure.

III. DESIGN AND BANDPASS NGD ANALYSIS OF "lill"-SHAPE MICROSTRIP CIRCUIT

The present section describes the BP NGD analysis of a particular ''lill'' shape NGD microstrip circuit. The design method of the circuit is described. Then, the measured S-parameters are discussed in order to determine its BP NGD specifications.

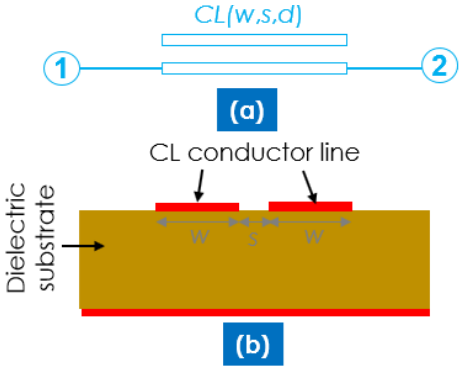

FIGURE 3. (a) Circuit diagram and (b) microstrip face view of two-port li-topology.

A. DESIGN OF THE PROOF OF CONCEPT (POC) LILL NGD CIRCUIT

After the introduction of the basic topology inspiring the lill-circuit design, the POC circuit is presented. Then, the experimental validation results of the BP NGD behavior are discussed.

1) ELEMENTARY TOPOLOGY LEADING TO INSPIRATION OF THE LILL-CIRCUIT

Fig. 3(a) represents the circuit diagram of the ''li'' topology [22]. It acts as one of the elementary NGD topology which can built with a single CL. This circuit is essentially composed of two identical parallel TLs. As illustrated by Fig. 3(b), the li-topology can be implemented with a CL, $CL(w, s, d)$, assumed as microstrip lines with a physical width w, a physical space, s, and a physical length, d.

One of the constituting li lines is open-ended at their two extremities. The other line is connected to the access ports. In consequence, the li-topology can be modelled with S-matrix system as shown in Fig. 1.

2) CONSTRUCTION OF LILL-CIRCUIT

For the case of li microstrip circuit with effective permittivity, ε_{reff}, the NGD center frequency can be defined with the equation [22]:

$$f_0 = \frac{c_0}{2d\sqrt{\varepsilon_{reff}}} \tag{17}$$

where c_0 is the speed of electromagnetic waves in vacuum. To synthesize a circuit with significant value of NGD, we can design a structure with multi-coupled lines with several open-ended TL under coupling. The main solution in the present study is to design a multi-coupled microstrip line structure named lill circuit. Based on the combined superposition NGD effect of li structure, NGD effect with significant absolute value is expected to be generated.

The final NGD circuit can be optimized in function of the length of the constituting open-ended TL. The innovative lill-circuit under investigation was imagined from the exploitation of the li-topology. The microstrip circuit design of the POC in the environment of the electronic and RF/microwave circuit simulator ADS® from Keysight Technologies® is developed in the following subsection.

B. DESCRIPTION OF THE LILL-MICROSTRIP CIRCUIT PROTOYPE

During the design, the NGD specifications shown in Table 1 were fixed. Then, the POCs was designed in microstrip technology. The planar top view of the POC is displayed in Fig. 4(a). The circuit design was made by choosing the width w of each line corresponding to obtain a characteristic impedance theoretically equal to $Z_c = 50\Omega$ which can be determined with Linecalc calculator tool of ADS® software. The circuit was implemented on the Cu-metalized laminating double face of Duroid Roger3210® dielectric substrate.

TABLE 1. Targeted NGD specifications.

Designation	*Center frequency*	*NGD value*	*Attenuation*
Parameter	f_0	GD_n	A
Value	2.3 GHz	-8 ns	-6 dB

The substrate physical characteristics are addressed in Table 2. The final circuit sizes were defined after optimization in ADS® environment. The photograph of the fabricated lill-circuit prototype is exposed in Fig. 4(b). The microstrip circuit prototype presents physical size, 33.2 mm × 14 mm respectively.

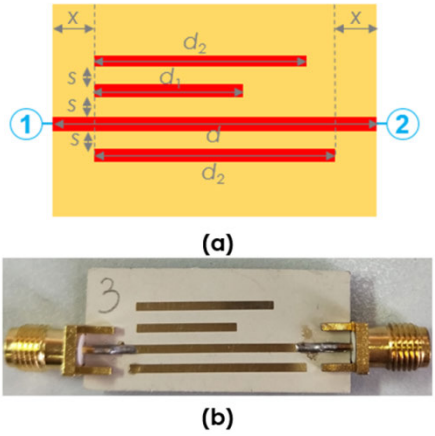

FIGURE 4. Photograph of the fabricated lill-circuit prototype.

TABLE 2. lill-circuit parameters and specifications.

Components	*Description*	*Parameter*	*Value*
Substrate	Material	Rogers3210	-
	Relative permittivity	ε_r	10.2
	Loss tangent	tan(δ)	0.003
	Thickness	h	1.27 mm
Metallization conductor	Material	Copper (Cu)	-
	Thickness	t	35 µm
	Conductivity	σ	58 MS/m
TL	Width	w	1.09 mm
	Length	d	33.2 mm
	Length	d_1	13.2 mm
	Length	d_2	18.2 mm
	Length	d_3	23.2 mm
Space	-	x	5.2 mm
	-	s	1.72 mm

C. DISCUSSION ON THE FREQUENCY DOMAIN VALIDATION RESULTS

The validation of the lill-circuit is explored in the present subsection. The experimental setup is briefly introduced. Then, the measured results of GD are discussed with respect to the BP NGD aspect.

1) EXPERIMENTAL SETUP WITH S-PARAMETER MEASUREMENT

The GD measurement of the lill circuit was carried out indirectly based on the S-parameters. Fig. 5 highlights the illustrative diagram of the performed experimental setup. The measured data of two-dimension S-parameters were recorded in touchstone format. Similar to classical microwave two-port circuits, the measurement was carried out on a two-port Vector Network Analyzer (VNA).

The frequency domain experimental test was realized with a VNA Rohde & Schwarz® referenced ZVA 24 working from 10 MHz to 24 GHz. The measured GD of the tested circuit was extracted from transmission parameter following

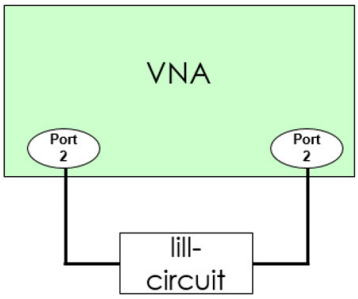

FIGURE 5. Illustrative diagram of the S-parameters experimental setup.

equation (5). The measured results are discussed in the following paragraphs.

2) DISCUSSION ON THE MEASURED GD AND S-PARAMETERS OF THE LILL CIRCUIT

The frequency domain validation of the BP NGD behavior of lill-circuit photographed in Fig. 4(b) is based on the S-parameter measurement. The test of the circuit was carried out in the frequency band between $f_{min} = 2$ GHz and $f_{max} = 2.8$ GHz. Figs. 6 display the measured GD of the lill-circuit shown in Fig. 5(b). As expected, the GD response confirms the BP NGD behavior. Furthermore, the "V"-shape behavior of BP NGD transmission coefficient proposed in Fig. 7(a) has been found as verified generally with many passive NGD circuits [8]–[20], [22]–[25]. The associated reflection coefficient is plotted in Fig. 7(b). Table 3 presents the comparison of measured NGD specifications.

TABLE 3. Measured lill-circuit NGD specifications.

Approach	f_0	$GD(f_0)$	BW	$S_{21}(f_0)$
Meas.	2.303 GHz	-8.1 ns	27 MHz	-6.66 dB

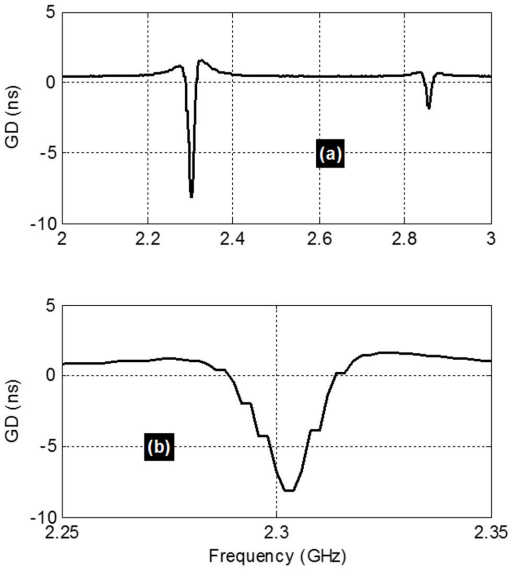

FIGURE 6. Measured GD of the lill-circuit photographed in Fig. 4(a): (a) wide and (b) narrow band plots.

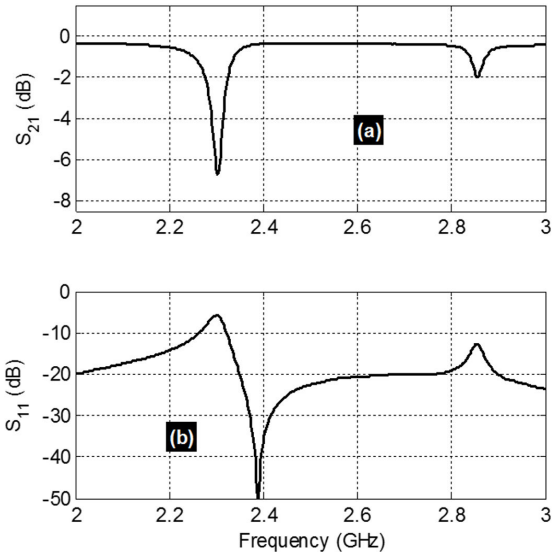

FIGURE 7. Measured (a) transmission and (b) reflection coefficients of the lill-circuit photographed in Fig. 4(b).

D. DISCUSSION ON THE BP NGD PERFORMANCE OF THE PROPOSED CIRCUIT

In order to quantify more clearly the contribution of the present NGD design in the frequency domain, we traditionally deal with what was done previously. Based on the proposition in the previous work, the NGD performance is also assessed with the NGD figure-of-merit (FOM), which is defined in [18], [24] formulated by:

$$FOM = |GD(f_0)| \times BW \times |S_{21}(f_0)| \tag{18}$$

Accordingly, a comparative study of the BP NGD performance of the proposed lill circuit with respect to the existing ones is examined in the present subsection. As addressed in Table 4, the comparison of the NGD performances of typical dual-band NGD function is recapitulated based on the research work available in the literature [18]–[19], [24], [35]. In this table, the first and second NGD center frequencies are denoted by f_1 and f_2, respectively. It can be pointed out from this table that the lill NGD circuit presents the following general benefits:

- Considerable fully distributed elements without lossy lumped component,
- Significant NGD absolute value,
- And a wide NGD FOM.

However, the lill circuit has weakness in term of reflection coefficient in the first NGD band.

To validate more convincingly the meaning of the BP NGD function, time-domain investigation is innovatively discussed in the following section.

IV. TIME-DOMAIN INVESTIGATION OF THE BP NGD FUNCTION AND TRANSIENT SIMULATIONS WITH THE LILL-CIRCUIT MODEL

To verify using a more practical way the frequency domain result of the previous section, the present section deals with the temporal validation. After the experimental setup description, the behavior of the output transient signal with respect to the input one is analyzed.

TABLE 4. Performance comparison.

References	f (GHz)	GD (ns)	S_{21}(dB)	S_{11}(dB)	FOM
[18]	f_1=3.5	-4.54	-47.4	-	0.0023
	f_2=5.15	-4.2	-38.8	-	0.0048
[19]	f_1=0.667	-1.19	-18.2	-24.8	0.0338
	f_2=1.377	-1.19	-18.2	-24.7	0.0332
[24]	f_1=2.436	-4.06	-2.13	-12.61	0.0381
	f_2=3.022	-3.83	-2.86	-12.40	0.0358
[35]	f_1=2.14	-3	-34.2	-17	0.0150
	f_2=3.5	-3.1	-34.9	-17	0.0100
This paper	f_1=2.303	-8.1	-6.66	-5.78	0.1016
	f_2=2.86	-1.84	-1.82	-12.7	0.0298

A. GENERAL DESCRIPTION ON THE BP NGD ANALYSIS IN THE TIME-DOMAIN

The expectation of the time-domain investigation of BP NGD circuit is the preliminarily introduced in the present subsection. The main characteristics of the input signal in function of the GD response is described. Then, the configuration of the input and the NGD circuit interaction is illustrated.

1) SYSTEMIC PRESENTATION OF THE TIME-DOMAIN RESPONSE

At the beginning of this analysis, the S-parameter model of the circuit under study can be used as a black box system. Fig. 8 represents the diagram of the time-domain configuration of the BP NGD analysis. In this diagram, the system is excited by t-time dependent or transient input signal, $v_{in}(t)$. Then, the transient output signal, $v_{out}(t)$, needs to be recorded simultaneously with the input. It is assumed that the output load of the terminal receiver (oscilloscope) is equal to the reference impedance, $R = R_0 = 50\Omega$.

FIGURE 8. Illustrative diagram to generate the time-domain response of system $S(j\omega)$.

It is noteworthy that the BP NGD time-domain analysis depends inevitably to the GD frequency domain response. The frequency domain analysis of the input signal can be performed following the hereafter golden rules.

- The input test signal spectrum written as:

$$V_{in}(\omega) = |fft\,[v_{in}(t)]|\,. \tag{19}$$

must be limited in bandwidth.

- The power spectrum of this test signal must belong to the NGD frequency band to operate with the NGD function. It is possible to choose for example the input signal power spectrum bandwidth, B, in function of the NGD bandwidth, Δf.
- The attenuation of the input signal spectrum at the NGD cut-off frequencies, ω_k, (with $k = 1, 2$) defined as:

$$\zeta_{dB} = 20 \log \left\{ \frac{V_{in}(\omega_k)}{\max\left[V_{in}(\omega)\right]} \right\} \tag{20}$$

must be chosen under the condition:

$$\zeta_{dB} \leq -10\ dB \tag{21}$$

in order to limit power outside NGD bandwidth.

This time-domain BP NGD study consists also in investigating on the behavior of the envelopes of input and output signals, Env[v_{in}(t)], and Env[v_{out}(t)], respectively.

2) ADOPTED PRINCIPLE OF THE TIME-DOMAIN BP NGD ANALYSIS

The practical principle of the present time-domain analysis of the BP NGD microwave circuit or microwave device requires the following conditions:

- the input must be pulse signal with limited duration,
- the input signal must be limited bandwidth and smoothed enough in the time-domain,
- an input signal with spectrum density essentially belonging in the NGD bandwidth,
- the input signal must be a modulated sine carrier having a carrier frequency equal NGD central frequency,
- and possibility to visualize simultaneously the input and output signals, v_{in} and v_{out}, respectively.

To translate the BP analysis in the time-domain, we have to pay a special attention on the delay between the input and output signal envelopes.

3) IDEAL CONFIGURATION OF THE TIME-DOMAIN EXPERIMENTATION OF BP NGD ANALYSIS

To satisfy this requirement, the proposed innovative solution is to use an arbitrary signal generator able to generate UWB or short duration pulsation signals. Then, it is very important also to record or to visualize the input and output simultaneously. Fig. 9 illustrates the experimental setup solution to address the challenging problem. This experimental setup constituted by double-output ($Out_{1,2}$) signal generator, the lill-circuit (as circuit under test) and terminated by a double-channel ($Ch_{1,2}$) oscilloscope. To make this configuration unrefutably efficient, the cables connecting Out_1-Ch_1 and Out_2-Ch_2 must be correctly identical.

The illustrative feasibility of the proposed methodology is explored in the next subsection with transient simulations of the lill-circuit.

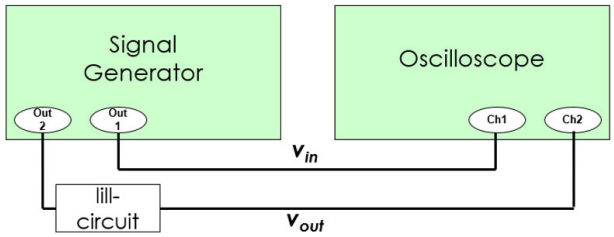

FIGURE 9. Illustrative diagram of the time-domain experimental setup with the NGD lill-circuit.

B. DISCUSSION ON THE TIME-DOMAIN SIMULATED RESULTS

An investigation by simulation constitutes an important step before the time-domain experimentation of BP NGD circuit. The present subsection introduces a preliminary numerical analysis with Gaussian responses injected to the lill-circuit. Different sine carrier frequencies will be considered to illustrate the responses of the S-parameters in and out of the NGD frequency band.

1) ANALYTICAL DEFINITION OF THE GAUSSIAN SIGNAL INPUT PULSE

Similarly to all microwave functions, the unfamiliar BP NGD circuit is expected to operate in a frequency band which is specified for BP NGD circuits by NGD bandwidth, Δf, containing the NGD center frequency, f_0. An ideal signal enabling to perform the time-domain characterization of BP NGD circuit should present:

- the possibility to limit the amplitude in function of the saturation of the NGD circuit and the test equipment's,
- the possibility of modulating a sine carrier with frequency equal to f_0,
- the possibility to limit the power spectrum bandwidth which means that the input signal envelope should be smoothed enough in function of the NGD bandwidth,
- and the possibility to compare the input signal leading and tailing edge or the signal optimal (minimal or maximal) peaks.

For this reason, in the present study, the chosen input signal is a Gaussian waveform modulating a sine carrier having a frequency equal to the NGD center frequency. The signal can be defined analytically by:

$$v_{in}(t) = e^{-\xi(t-t_0)^2} \sin(2\pi f_0 t) \tag{22}$$

with the maximal peak instant time, t_0, and gaussian time-width parameter, ξ, which must be calculated in function of the NGD bandwidth by the formula [34]:

$$\xi = \frac{-5\pi^2 B^2}{\zeta_{dB} \ln(10)}. \tag{23}$$

During the numerical application of present study, the considered Gaussian signals corresponding to input signal has a bandwidth, $B = 27$ MHz and $\zeta_{dB} = -10$ dB. The following paragraphs present ADS® transient simulation results with respect to the diagram configured in Fig. 8 after replacing the

black box by the measured touchstone S-parameter of the lill-circuit. Three cases of sine carrier frequency, $f_c = \{2.1$ GHz, 2.3 GHz, 2.5 GHz$\}$, have been intentionally proposed. The transient simulations were carried out over the time window with $t_{min} = 0$ and $t_{max} = 140$ ns.

2) TRANSIENT SIMULATION WITH GAUSSIAN INPUT PULSE MODULATING 2.1 GHz SINE CARRIER

Figs. 10(a) and Fig. 10(b) displays the input and output signals after ADS® simulation results with a Gaussian modulating a sine carrier having frequency, $f_c = 2.1$ GHz. If we look back in Figs. 6, the lill-circuit presents a positive GD of about 0.5 ns. Therefore, the output Gaussian of Fig. 10(b) present leading and tailing edges slightly delayed compared to the input ones. It is possible to interpret from this transient result that there is no BP NGD effect for this input signal.

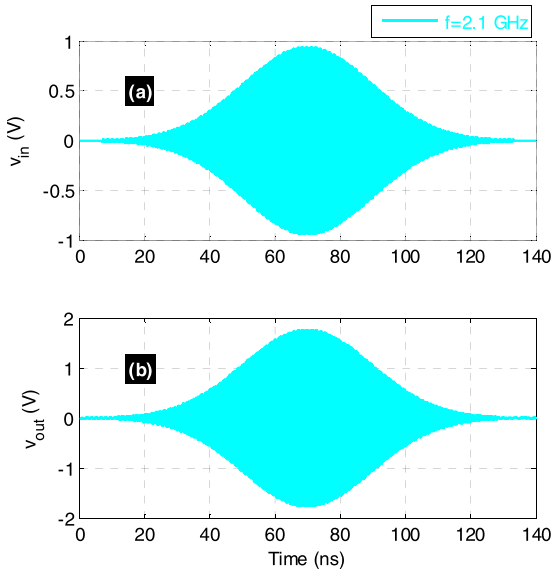

FIGURE 10. Time-domain simulation results of the lill-circuit touchstone S-parameter with Gaussian pulse input modulating, $f_c = 2.1$ GHz sine carrier.

3) TRANSIENT SIMULATION WITH GAUSSIAN INPUT PULSE MODULATING 2.3 GHz SINE CARRIER

A Gaussian input pulse modulating sine carrier frequency, $f_c = 2.3$ GHz, which is equal to the NGD center frequency of lill-circuit as shown in Figs. 6 is considered in this case of study. Accordingly, we obtain the fascinating transient simulation result plotted in Figs. 11.

It is possible to emphasize from Fig. 11(b) that the output is more significantly attenuated compared to the previous case of Gaussian input pulse modulating a sine carrier having a frequency $f_c = 2.1$ GHz. As expected, the output signal leading and tailing edges appear in time-advance compared to the input signal ones. This counterintuitive effect highlights essentially the signature of BP NGD function which depends on the NGD frequency band and NGD value as illustrated by the lill-circuit GD introduced in Figs. 6. The possibility to

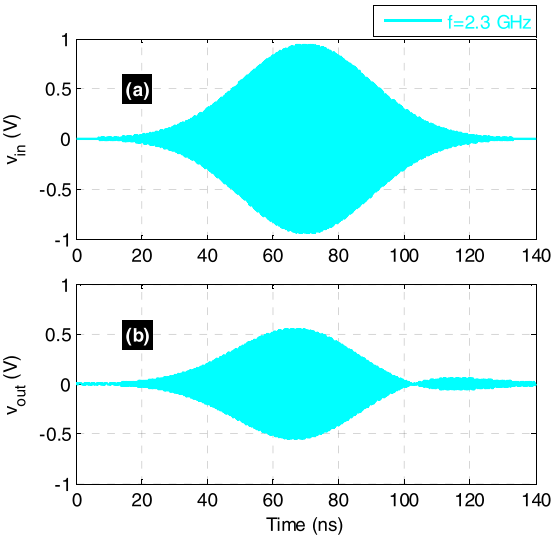

FIGURE 11. Time-domain simulation results of the lill-circuit touchstone S-parameter with Gaussian pulse input modulating $f_c = 2.3$ GHz sine carrier.

generate this transient behavior is due to the fact that the input signal spectrum bandwidth belongs to the lill-circuit NGD bandwidth.

4) TRANSIENT SIMULATION WITH GAUSSIAN INPUT PULSE MODULATING 2.5 GHz SINE CARRIER

This last case of transient simulation was carried out with Gaussian input pulse modulating sine carrier frequency, $f_c = 2.5$ GHz. The obtained result is shown in Figs. 12. We can understand visibly that this time-domain response is similar to the previous case of study with $f_c = 2.1$ GHz. It is then possible to underline that the absence of the signal advance can be explained by the positive GD almost equal to 0.5 ns around 2.5 GHz according the lill-circuit measured GD displayed in Figs. 6.

5) CONCLUSION FROM TRANSIENT SIMULATION INVESTIGATION

It can be partially concluded from the three cases of the transient simulation results that the distortion between the input and output signals waveform of the lill NGD circuit can be neglected. Nevertheless, the difference between the input and output can be assessed with the comparisons between the input ouput maximum amplitudes ratio:

$$a = \frac{\max(v_{in})}{\max(v_{out})} \tag{24}$$

and also, the instant time of the signal maximum peaks by the following equation:

$$\Delta t_{peak} = t_{out} - t_{in} \tag{25}$$

by taking:

$$\begin{cases} \max(v_{out}) = v_{out}(t_{out}) \\ \max(v_{in}) = v_{in}(t_{in}) \end{cases}. \tag{26}$$

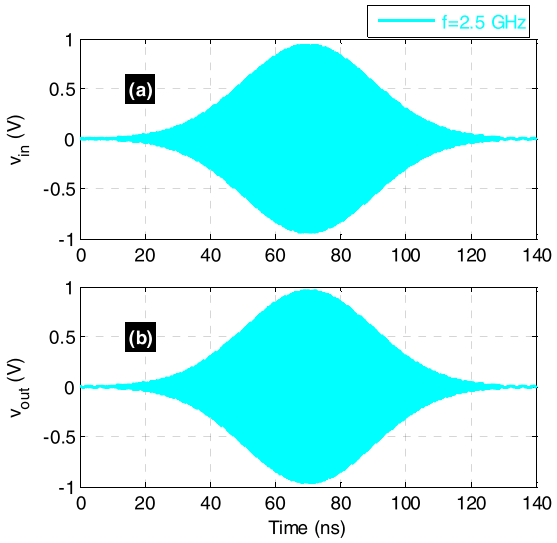

FIGURE 12. Time-domain simulation results of the lill-circuit touchstone S-parameter with Gaussian pulse input modulating $f_c = 2.5$ GHz sine carrier.

Table 5 summarizes the input and output maximal peak delay from the signals plotted in Figs. 10, Figs. 11 and Figs. 12.

TABLE 5. Comparison of input and output gaussian signal delays from simulated touchstone model of lill circuit.

Carrier frequency	a	Δt_{peak}
f_c=2.1 GHz	-0.4 dB	0.43 ns
f_c=2.3 GHz	-6.5 dB	-7.62 ns
f_c=2.5 GHz	-0.35 dB	0.43 ns

In conclusion of all the results, the output Gaussian pulse is susceptible to propagate through the lill-circuit with leading and tailing edge in time-advance if the input signal power spectrum belongs to the NGD frequency band shown in Figs. 6.

V. EXPERIMENTAL VALIDATION OF THE BP NGD FUNCTION WITH THE "lill" MICROSTRIP CIRCUIT IN THE TIME-DOMAIN

The ultimate time-domain validation of the BP NGD behavior of the lill-circuit prototype photographed in Fig. 4(b) is developed in the present section. The experimentation technique is described. Then, the NGD characterization based on the generation and measured Gaussian transient signals is discussed.

A. EXPERIMENTAL SETUP

The experimental setup of the lill-circuit time-domain measurement is studied in the present subsection. The visualization technique of the input and output signals is explained.

1) EXPERIMENTAL SETUP

The synthetic application of all the preliminary different steps of previous section leads us to settle the NGD experimentation following the illustrative diagram methodologically earlier depicted in Fig. 9. The main challenge of the experimentation is to visualize in correct manner the input and output signals simultaneously.

According to the simulation study of previous section, the BP NGD effect can be verified with Gaussian pulse. During the test, the ultra-wide band (UWB) microwave arbitrary signal generator referenced, Tektronix® AWG70001A having sampling rate equal to 50 GSps, 10 bits memory was employed. This generator is susceptible to deliver two perfectly synchronized opposite signals from channels A and B with time shift better than 5 ps. To plot the signals, the four-channel oscilloscope referenced Agilent® DSO81204A having a bandwidth of 12 GHz and a maximal sampling rate equal to 40 GSps was employed. As argued in the previous section, the oscilloscope was calibrated with input impedance, $Z_{in} = R_0 = 50\Omega$. Fig. 13 highlights the photograph of the experimental setup including the tested lill-circuit. During the experimentation test, the input port of the circuit was connected to the generator and the output port to one of the oscilloscope outputs through SMA connectors and 1 m-length cables.

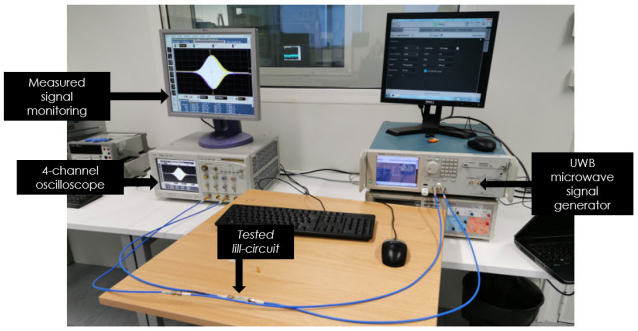

FIGURE 13. Photograph of the time-domain experimental setup with the NGD lill-circuit prototype.

Then, after the successful test, the obtained results were recorded attentively as data files saved in csv-format. After this data post-processing, we obtained the measured results discussed in the following subsection.

B. DISCUSSION ON THE BP NGD MEASURED USING THE TRANSIENT EXPERIMENTAL SETUP WITH INPUT GAUSSIAN WAVEFORM PULSE

The ultimate BP NGD time-domain measurement of the lill-circuit was successfully carried out with a Gaussian pulse signal. This input pulse was generated in order to obtain a signal presenting the analytical specifications addressed in Table 6. It is crucial during the test that the input signal power spectrum is tuned to be interleaved within the NGD frequency band. For this reason, the NGD time-domain experimentation must absolutely preceded by frequency domain analysis in order to confirm the NGD specifications as aforementioned in Section II via the ideal NGD response depicted in Figs. 2.

It should be kept in mind with particular attention of the researcher assisted generally by the technicians or the students during the measurement campaign that the output signal appears in time-advance compared to the input.

TABLE 6. Specifications of the tested input signal.

Specifications	Description	Value
Amplitude	V_{max}	170 mV
Sine carrier frequency	f_c	2.310 GHz
Peak instant time	t_0	70 ns
Bandwidth parameter	ζ	-10 dB
Bandwidth	B	27 MHz

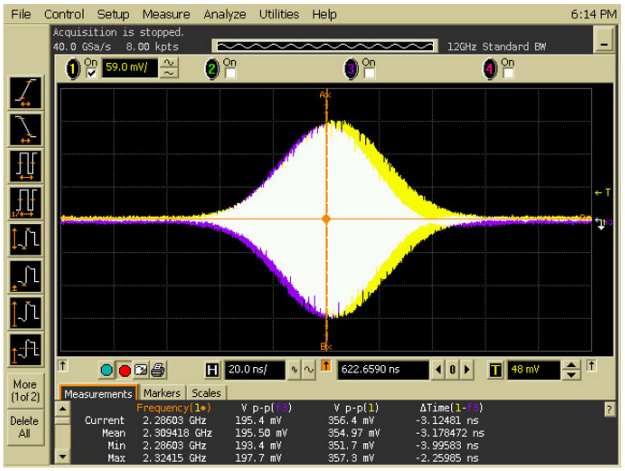

FIGURE 14. Oscilloscope screen snapshot of the measured signals.

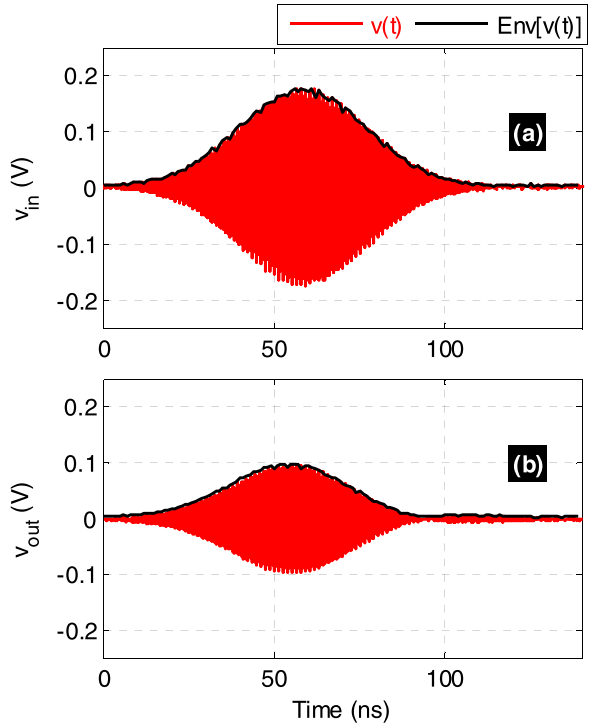

FIGURE 15. Measured transient plots of the compared Gaussian input and output signal envelopes of the lill-circuit: (a) natural and (b) normal plots.

During this BP NGD experimental test, we snapshotted in Fig. 14, the simultaneous plots of measured input and output measured signals which can be attentively commented as follows.

- In this picture, the yellow curve represents the input signal. It represents a Gaussian signal as expected in the previous specifications.
- The purple curve represents the output signal, the white curve representing the part where the input and the output signals are superimposed.
- This output signal was rescaled in order to highlight the output signal advance compared to the input.
- At this stage of experimental study, we successfully demonstrate the BP NGD behavior of the lill-circuit in the time-domain.

To highlight more analytically, the expected BP NGD effect, these two signals were recorded in csv-format data file in an USB socket from the Agilent® DSO81204A digital oscilloscope. Further post-processing of the obtained data performed in the MATLAB® environment gives the transient results displayed finally in Figs. 15. In these plots, the input and output measured transient signals are plotted in red curves of Fig. 15(a) and Fig. 15(b), respectively.

In order to evaluate the BP NGD specifications, further post-processing was performed for the extraction of the input and output signal envelopes. We can see both in Fig. 15(a) and Fig. 15(b) that the extracted envelopes which are plotted in black curves fit perfectly with the natural transient signals. The next last subsection assesses the time-domain BP NGD performance from the envelope signal analysis.

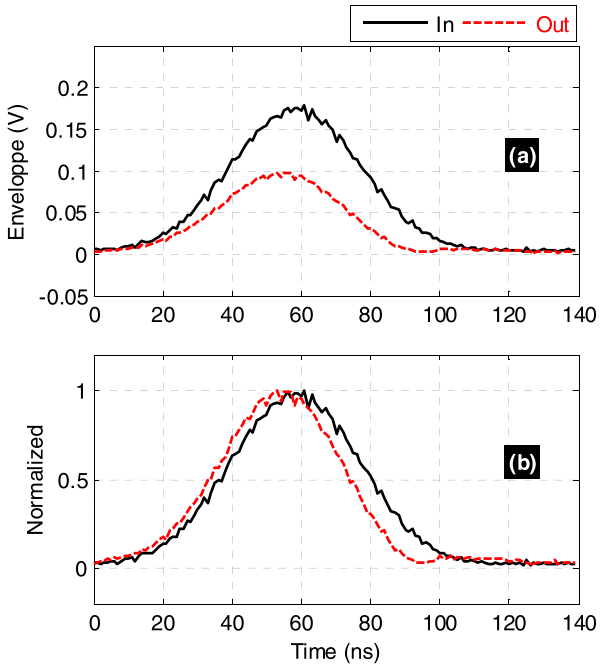

FIGURE 16. Measured envelopes of the compared Gaussian input and output signal envelopes of the lill-circuit: (a) natural and (b) normal plots.

C. ANALYSIS OF THE BP NGD RESPONSE SIGNAL ENVELOPE

Fig. 16(a) represents the plot of the main objective of the BP NGD aspect of the lill-circuit in a nutshell of the whole study.

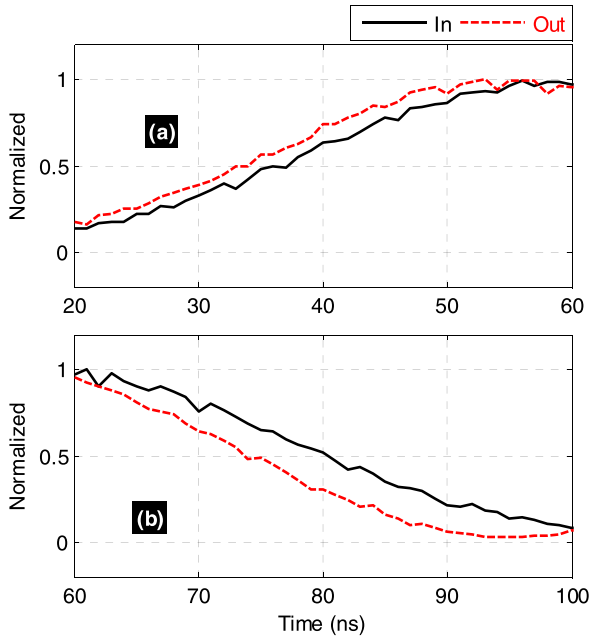

FIGURE 17. Zoom in of (a) leading and (b) tailing edges of measured input and output normalized transient signals shown in Fig. 16(b).

These input and output measured transient signals which are displayed in black and red curves, respectively are obtained from the test photographed in Fig. 13. We can emphasize as predicted in simulation of previous section that the output is notably attenuated compared with the input. In order to demonstrate more clearly, the BP NGD function inherently appropriated to the lill-circuit of Figs. 4 from the time-domain investigation, the input and output signals are unity-normalized plotted again in Fig. 16(b). The extraordinary and difficult to believe time-advance of the output signal fronts was also illustrated. Moreover, despite the inevitably noise affecting the measured signals, the input and output of the lill-circuit remain very well-correlated with almost negligible distortion. The answer can be understood from the comparison between the input ones are explained more irrefutably in the zoom in plots of Fig. 17(a) and Fig. 17(b). The quantitative measurement results of the BP NGD specification are recapitulated in Table 7.

TABLE 7. Comparison of input and output signal delays from simulated touchstone model of lill-circuit.

Specifications	Description	Value
Absolute rise time advance	Δt_{rise}	-5.1 ns
Absolute fall time advance	Δt_{fall}	-7.6 ns
Voltage attenuation	a	0.57
Correlation coefficient	$corr(V_{in}, V_{out})$	95 %

VI. CONCLUSION

An original experimental investigation on the BP NGD function is developed. The basic theory of the BP NGD function is addressed based on the S-matrix of a two-port circuit. The ideal response diagram of BP NGD response is presented. The main specifications enabling to the electronic engineers to define the objective of the BP NGD circuit design are explained quantitatively.

To concretize the BP NGD theory, the design of innovative passive topology of lill-circuit is described. The implementation of the microstrip circuit in function of the available substrate specifications is introduced. The BP NGD behavior of the lill-circuit was validated with S-parameter measurement. As expected, NGD function with 2.3 GHz NGD center frequency with about −8 ns NGD value is obtained.

The time-domain validation of the lill-circuit prototype was performed. An innovative experimentation technique is described based on an UWB arbitrary signal generator and allows the possibility to plot the input and output signals simultaneously. The considered waveform test signal is a Gaussian pulse modulating a sine carrier. As expected, output signals with leading, trailing and peak in advance compared to the input ones are observed.

The present research results open the new possibilities of testing BP NGD applications notably in the microwave communication engineering as expected in [1]–[5].

REFERENCES

[1] A. Mortazawi and W. Alomar, "Negative group delay circuit," U.S. Patent 20 160 093 958, Mar. 2016.
[2] H. Mirzaei and G. V. Eleftheriades, "Realizing non-foster reactive elements using negative-group-delay networks," *IEEE Trans. Microw. Theory Techn.*, vol. 61, no. 12, pp. 4322–4332, Dec. 2013.
[3] T. Zhang, R. Xu, and C.-T.-M. Wu, "Unconditionally stable non-foster element using active transversal-filter-based negative group delay circuit," *IEEE Microw. Wireless Compon. Lett.*, vol. 27, no. 10, pp. 921–923, Oct. 2017.
[4] B. Ravelo, S. Lalléchère, A. Thakur, A. Saini, and P. Thakur, "Theory and circuit modeling of baseband and modulated signal delay compensations with low- and band-pass NGD effects," *AEU-Int. J. Electron. Commun.*, vol. 70, no. 9, pp. 1122–1127, Sep. 2016.
[5] T. Shao, Z. Wang, S. Fang, H. Liu, and Z. N. Chen, "A full-passband linear-phase band-pass filter equalized with negative group delay circuits," *IEEE Access*, vol. 8, pp. 43336–43343, Feb. 2020.
[6] B. Segard and B. Macke, "Observation of negative velocity pulse propagation," *Phys. Lett. A*, vol. 109, no. 5, pp. 213–216, May 1985.
[7] B. Macke and B. Ségard, "Propagation of light-pulses at a negative group-velocity," *Eur. Phys. J. D, At., Mol. Opt. Phys.*, vol. 23, no. 1, pp. 125–141, Apr. 2003.
[8] G. V. Eleftheriades, O. Siddiqui, and A. K. Iyer, "Transmission line models for negative refractive index media and associated implementations without excess resonators," *IEEE Microw. Wireless Compon. Lett.*, vol. 13, no. 2, pp. 51–53, Feb. 2003.
[9] O. F. Siddiqui, M. Mojahedi, and G. V. Eleftheriades, "Periodically loaded transmission line with effective negative refractive index and negative group velocity," *IEEE Trans. Antennas Propag.*, vol. 51, no. 10, pp. 2619–2625, Oct. 2003.
[10] C. D. Broomfield and J. K. A. Everard, "Broadband negative group delay networks for compensation of oscillators, filters and communication systems," *Electron. Lett.*, vol. 36, no. 23, pp. 1931–1933, Nov. 2000.
[11] L.-F. Qiu, L.-S. Wu, W.-Y. Yin, and J.-F. Mao, "Absorptive bandstop filter with prescribed negative group delay and bandwidth," *IEEE Microw. Wireless Compon. Lett.*, vol. 27, no. 7, pp. 639–641, Jul. 2017.
[12] R. Gomez-Garcia, J.-M. Munoz-Ferreras, W. Feng, and D. Psychogiou, "Input-reflectionless negative-group-delay bandstop-filter networks based on lossy complementary duplexers," in *IEEE MTT-S Int. Microw. Symp.*, Boston, MA, USA, Jun. 2019, pp. 1031–1034.
[13] Z. Wang, Y. Cao, T. Shao, S. Fang, and Y. Liu, "A negative group delay microwave circuit based on signal interference techniques," *IEEE Microw. Wireless Compon. Lett.*, vol. 28, no. 4, pp. 290–292, Apr. 2018.

[14] M. A. Sanchez-Soriano, J. Dura, S. Sirci, and S. Marini, "Signal-interference-based structure with negative group delay properties," in *Proc. 48th Eur. Microw. Conf. (EuMC)*, Madrid, Spain, Sep. 2018, pp. 1021–1024.
[15] C.-T.-M. Wu and T. Itoh, "Maximally flat negative group-delay circuit: A microwave transversal filter approach," *IEEE Trans. Microw. Theory Techn.*, vol. 62, no. 6, pp. 1330–1342, Jun. 2014.
[16] G. Liu and J. Xu, "Compact transmission-type negative group delay circuit with low attenuation," *Electron. Lett.*, vol. 53, no. 7, pp. 476–478, Mar. 2017.
[17] T. Shao, Z. Wang, S. Fang, H. Liu, and S. Fu, "A compact transmission-line self-matched negative group delay microwave circuit," *IEEE Access*, vol. 5, pp. 22836–22843, Oct. 2017.
[18] G. Chaudhary, Y. Jeong, and J. Lim, "Miniaturized dual-band negative group delay circuit using dual-plane defected structures," *IEEE Microw. Wireless Compon. Lett.*, vol. 21, no. 1, pp. 19–21, Jan. 2011.
[19] T. Shao, S. Fang, Z. Wang, and H. Liu, "A compact dual-band negative group delay microwave circuit," *Radioengineering*, vol. 27, no. 4, pp. 1070–1076, Dec. 2018.
[20] M. Kandic and G. E. Bridges, "Asymptotic limits of negative group delay in active resonator-based distributed circuits," *IEEE Trans. Circuits Syst. I, Reg. Papers*, vol. 58, no. 8, pp. 1727–1735, Aug. 2011.
[21] B. Ravelo, "Similitude between the NGD function and filter gain behaviours," *Int. J. Circuit Theory Appl.*, vol. 42, no. 10, pp. 1016–1032, Oct. 2014.
[22] B. Ravelo, L. Wu, F. Wan, W. Rahajandraibe, and N. M. Murad, "Negative group delay theory on li topology," *IEEE Access*, vol. 8, pp. 47596–47606, Mar. 2020.
[23] F. Wan, B. Liu, P. Thakur, A. Thakur, S. Lalléchère, W. Rahajandraibe, and B. Ravelo, "0IO-shape PCB trace negative group-delay analysis," *IEEE Access*, vol. 8, pp. 2169–3536, Dec. 2020.
[24] X. Zhou, B. Li, N. Li, B. Ravelo, X. Hu, Q. Ji, F. Wan, and G. Fontgalland, "Analytical design of dual-band negative group delay circuit with multi-coupled lines," *IEEE Access*, vol. 8, pp. 72749–72756, Apr. 2020.
[25] W. Jian-Wu and F. Zheng-He, "Time-domain nature of group delay," *Chin. Phys. B*, vol. 24, no. 10, pp. 1–5, 2015.
[26] F. Wan, N. Li, B. Ravelo, J. Ge, and B. Li, "Time-domain experimentation of NGD ActiveRC-network cell," *IEEE Trans. Circuits Syst. II, Exp. Briefs*, vol. 66, no. 4, pp. 562–566, Apr. 2019.
[27] H. Wang, C. Zhuang, R. Zeng, S. Xie, and J. He, "Transient voltage measurements for overhead transmission lines and substations by metal-free and contactless integrated electro-optic field sensors," *IEEE Trans. Ind. Electron.*, vol. 66, no. 1, pp. 571–579, Jan. 2019.
[28] S. Prakash, H. Martinez-Garcia, M. H. Naderi, H. Lee, and J. Silva-Martinez, "An agile supply modulator with improved transient performance for power efficient linear amplifier employing envelope tracking techniques," *IEEE Trans. Power Electron.*, vol. 35, no. 4, pp. 4178–4191, Apr. 2020.
[29] B. Couraud, T. Deleruyelle, E. Kussener, and R. Vauche, "Real-time impedance characterization method for RFID-type backscatter communication devices," *IEEE Trans. Instrum. Meas.*, vol. 67, no. 2, pp. 288–295, Feb. 2018.
[30] B. Thors, A. Furuskar, D. Colombi, and C. Tornevik, "Time-averaged realistic maximum power levels for the assessment of radio frequency exposure for 5G radio base stations using massive MIMO," *IEEE Access*, vol. 5, pp. 19711–19719, 2017.
[31] K. R. Foster, M. C. Ziskin, Q. Balzano, and A. Hirata, "Thermal analysis of averaging times in radio-frequency exposure limits above 1 GHz," *IEEE Access*, vol. 6, pp. 74536–74546, Nov. 2018.
[32] S. Bourdel, Y. Bachelet, J. Gaubert, R. Vauche, O. Fourquin, N. Dehaese, and H. Barthelemy, "A 9-pJ/pulse 1.42-vpp OOK CMOS UWB pulse generator for the 3.1–10.6-GHz FCC band," *IEEE Trans. Microw. Theory Techn.*, vol. 58, no. 1, pp. 65–73, Jan. 2010.
[33] R. Vauche, E. Muhr, O. Fourquin, S. Bourdel, J. Gaubert, N. Dehaese, S. Meillere, H. Barthelemy, and L. Ouvry, "A 100 MHz PRF IR-UWB CMOS transceiver with pulse shaping capabilities and peak voltage detector," *IEEE Trans. Circuits Syst. I, Reg. Papers*, vol. 64, no. 6, pp. 1612–1625, Jun. 2017.
[34] R. Vauche, S. Bourdel, N. Dehaese, J. Gaubert, O. Ramos Sparrow, E. Muhr, and H. Barthelemy, "High efficiency UWB pulse generator for ultra-low-power applications," *Int. J. Microw. Wireless Technol.*, vol. 8, no. 3, pp. 495–503, May 2016.

RÉMY VAUCHÉ (Member, IEEE) received the M.Eng. degree in microelectronics and telecommunication from Polytech' Marseille, Marseille, France, in 2008, the M.S. degree in microelectronics and nanoelectronics from Aix-Marseille University, Marseille, in 2008, and the Ph.D. degree in microelectronics from the University of Provence, Marseille, in 2011.

From 2011 to 2014, he was a Lecturer and a Researcher with the ISEN French Engineering School, Toulon, France. Since 2014, he has been an Associate Professor with Aix-Marseille University. His current research interests include the design of integrated circuits and systems for ultra-wideband impulse radio, human body communications, and home-care applications. He is currently a member of the Integrated Circuits Design Team, Provence Nanosciences Microelectronics and Materials Laboratory, Marseille.

RYM ASSILA BELHADJ MEFTEH received the B.S. degree in embedded electronics from the University of Carthage, Tunis, Tunisia, in 2016, the M.S. degree in industrial systems control from the University of Tunis Carthage, in 2017, and the M.S. degree in embedded electronics from the University of Lorraine, Nancy, France, in 2019. She is currently pursuing the Ph.D. degree in microelectronics with the University of Aix-Marseille.

Her current research interests include the design of emitters and receivers to estimate in real-time the link budget of human body communications and the design of HBC emitter front-end to guarantee limitations in terms of emitted spectrum and emitted power.

FAYROUZ HADDAD (Member, IEEE) received the master's degree in electronic engineering from ENSEIRB, Bordeaux, France, in 2006, and the Ph.D. degree in microelectronics from Aix-Marseille University, France, in 2009.

Since 2010, she joined the Integrated Circuits Design team, Institute of Materials, Microelectronics and Nanosciences of Provence (IM2NP), Marseille, France. She is currently an Assistant Professor with Aix-Marseille University (AMU). She co-organized the International Conferences ICECS 2014 and NEWCAS 2021, and also was a member of the technical program committee of several IEEE international conferences. She is a reviewer of IEEE TRANSACTIONS ON CIRCUITS AND SYSTEMS (TCAS), *International Journal of Electronics and Communications* (AEUE), *Applied Sciences* journal, *Electronics Letters* (IET), and so on, as well as for many IEEE conferences dedicated to integrated circuits (ISCAS, NEWCAS, ICECS, MWSCAS, ICMCS, and SBCCI). She co-supervised five Ph.D. and eight Master students. She is the author or coauthor of more than 70 articles published in referred journals and conferences. Her research interests include CMOS analog and RF integrated circuits design, ultra-low power (ULP), and multi-standards applications.

JAMEL NEBHEN (Member, IEEE) received the M.Sc. degree in microelectronics from the National Engineering School of Sfax, Tunisia, in 2007, and the Ph.D. degree in microelectronics from Aix-Marseille University, France, in 2012. From 2012 to 2018, he worked as a Postdoctoral Researcher in France in LIRMM-Lab Montpellier, IM2NP-Lab Marseille, ISEP Paris, LE2I-Lab Dijon, Lab-Sticc Telecom Bretagne Brest, and IEMN-Lab Lille. Since 2019, he joined the Prince Sattam Bin Abdulaziz University, Al-Kharj, Saudi Arabia, as an Assistant Professor. His research interests include the design of analog and RF integrated circuits, the IoT, biomedical circuit, and sensors instrumentation.

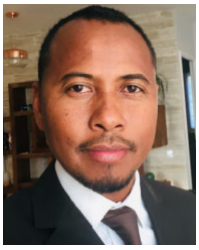

WENCESLAS RAHAJANDRAIBE (Member, IEEE) received the B.Sc. degree in electrical engineering from Nice Sophia-Antipolis University, France, in 1996, the M.Sc. degree (Hons.) in electrical engineering from the Science Department, University of Montpellier, France, in 1998, and the Ph.D. degree in microelectronics from the University of Montpellier. Since 1998, he has been joined the Informatics, Robotics and Microelectronics Laboratory of Montpellier (LIRMM), Microelectronics Department. Since 2003, he has also been joined the Materials, Microelectronics and Nanoscience Laboratory of Provence (IM2NP), Microelectronic Department, Marseille, France, where he was an Associate Professor. Since 2014, he has been a Professor with Aix Marseille University, where he heads the Integrated Circuit Design Group of the IM2NP Laboratory. He is currently a Full Professor with the University of Aix-Marseille. He is regularly involved to participate and to lead national and international research projects (ANR, H2020, and FP7 KIC-InnoEnergy). He directed and co-supervised 18 Ph.D. and 15 Master students. He is the author or coauthor of 11 patents and more than 150 articles published in refereed journals and conferences. He is an Expert for the ANR, the French Agency for Research. He has served on program committees for IEEE NEWCAS and ICECS. He has been and is a reviewer of contributions submitted to several IEEE conferences and journals, such as ISCAS, NEWCAS, MWSCAS, ESSCIRC, ESSDERC, RFIC, IEEE TRANSACTIONS ON CIRCUITS AND SYSTEMS—I: REGULAR PAPERS, IEEE TRANSACTIONS ON CIRCUITS AND SYSTEMS—II: EXPRESS BRIEFS, and IET *Electronics Letters*. His research interests include AMS and RF circuit design from transistor to architectural level. His current research interests include ultralow power circuit design for smart sensor interface and embedded electronic in bioelectronic and e-health applications, wireless systems, and design technique and architecture for multi-standard transceiver.

FAYU WAN (Member, IEEE) received the Ph.D. degree in electronic engineering from the University of Rouen, Rouen, France, in 2011. From 2011 to 2013, he was a Postdoctoral Fellow with the Electromagnetic Compatibility Laboratory, Missouri University of Science and Technology, Rolla. He is currently a Full Professor with the Nanjing University of Information Science & Technology, Nanjing, China. His current research interests include negative group delay circuits, electrostatic discharge, electromagnetic compatibility, and advanced RF measurement.

SÉBASTIEN LALLÉCHÈRE (Member, IEEE) received the Ph.D. degree in electronics and electromagnetics from Université Blaise Pascal (UBP), Clermont-Ferrand, France, in 2006, and the French "Habilitation à Diriger des Recherches" (HDR) degree from Universté Clermont Auvergne (UCA), Clermont-Ferrand, in 2018. He has served as a Research Engineer for LASMEA, Clermont-Ferrand, in 2007, focusing on intensive computational methods for electromagnetics. He joined UBP as an Assistant Professor in September 2007. He has been an Associate Professor with Université Clermont Auvergne (UCA) since 2017, and the Institut Pascal since 2012. His research interests include electromagnetic compatibility (EMC), antennas and propagation, complex systems, computational electromagnetics, reliability, stochastic, and sensitivity analysis for electrical engineering issues. He is actively involved in different research projects in antennas, RF, and EMC. Since 2019, he has also been the Head of the French URSI Commission E "EM environment and interferences."

BLAISE RAVELO (Member, IEEE) is currently the University Full Professor with NUIST, Nanjing, China. His research interests include multiphysics and electronics engineering. He is a pioneer of the negative group delay (NGD) concept about t<0 signal travelling physical space. This extraordinary concept is potentially useful for anticipating and prediction all kind of information. He was the research director of 11 Ph.D. students (seven defended), postdocs, research engineers, and Master internships. With US, Chinese, Indian, European, and African partners, he is actively involved and contributes on several international research projects (ANR, FUI, FP7, INTERREG, H2020, Euripides^2, and Eurostars). He is also a member of IET *Electronics Letters* editorial board as the Circuit & System Subject Editor. He is also a member of scientific technical committee of Advanced Electromagnetic Symposium (AES) 2013. His Google scholar H-index since 2020. He is also a member of research groups: IEEE, URSI, GDR Ondes, Radio Society and (co) authors of more than 330 scientific research articles in new technologies published in international conferences and journals. He is also a Lecturer of circuit & system theory, STEM (science, technology, engineering and maths), and applied physics. He is regularly invited to review articles submitted for publication to international journals (IEEE TRANSACTIONS ON MICROWAVE THEORY AND TECHNIQUES, IEEE TRANSACTIONS ON CIRCUITS AND SYSTEMS, IEEE TRANSACTIONS ON ELECTROMAGNETIC COMPATIBILITY, IEEE TRANSACTIONS ON INDUSTRIAL ELECTRONICS, IEEE ACCESS, *IET Circuits, Devices & Systems (CDS)*, and *IET Microwaves Antennas & Propagation (MAP)*) and books (Wiley, and Intech Science).